Cement & Concrete Composites 55 (2015) 53–61

Contents lists available at ScienceDirect

Cement & Concrete Composites

journal homepage: www.elsevier.com/locate/cemconcomp

Effect of calcium sulfate source on the hydration of calcium sulfoaluminate eco-cement

Marta García-Maté [a], Angeles G. De la Torre [a], Laura León-Reina [b], Enrique R. Losilla [a], Miguel A.G. Aranda [a,c], Isabel Santacruz [a,*]

[a] Departamento de Química Inorgánica, Cristalografía y Mineralogía, Universidad de Málaga, 29071 Málaga, Spain
[b] Servicios Centrales de Investigación, Universidad de Málaga, 29071 Málaga, Spain
[c] ALBA-CELLS Synchrotron, Carretera BP 1413, Km. 3.3, 08290 Cerdanyola, Barcelona, Spain

ARTICLE INFO

Article history:
Received 24 February 2014
Received in revised form 26 June 2014
Accepted 9 August 2014
Available online 19 August 2014

Keywords:
LXRPD
Rietveld method
Impedance spectroscopy
Temperature
Rheology
Mechanical strength

ABSTRACT

The availability of cements, including eco-cements, with tailored mechanical properties is very important for special applications in the building industry. Here we report a full study of the hydration of calcium sulfoaluminate eco-cements with different sulfate sources (gypsum, bassanite and anhydrite) and two water/cement ratios (0.50 and 0.65). These parameters have been chosen because they are known to strongly modify the mechanical properties of the resulting mortars and concretes. The applied multi-technique characterization includes: phase assemblage by Rietveld method, evolved heat, conductivity, rheology, compressive strength and expansion/retraction measurements. The dissolution rate of the sulfate sources is key to control the hydration reactions. Bassanite dissolves very fast and hence the initial setting time of the pastes and mortars is too short (20 min) to produce homogeneous samples. Anhydrite dissolves slowly so, at 1 hydration-day, the amount of ettringite formed (20 wt%) is lower than that in gypsum pastes (26 wt%) ($w/c = 0.50$), producing mortars with lower compressive strengths. After 3 hydration-days, anhydrite pastes showed slightly larger ettringite contents and hence, mortars with slightly higher compressive strengths. Ettringite content is the chief parameter to explain the strength development in these eco-cements.

1. Introduction

The manufacture of Calcium SulfoAluminate (CSA) cements is more environmentally friendly than that of OPC [1–4] as their production releases up to 40% less CO_2 than the latter (this reduction depends on CSA composition). The main performances of CSA cements are fast setting time (followed by a rapid hardening), good-chemical resistance properties and, depending on the amount of the added sulfate source they are self-levelling materials or shrinkage controllers [5,6]. In addition, they show high early strengths, good impermeability, sulfate and chloride corrosion resistance and low alkalinity [7].

CSA cements present a wide range of phase assemblages, but all of them contain over 50 wt% calcium sulfoaluminate (also known as yéelimite, Klein's salt, $Ca_4Al_6SO_{16}$ or $C_4A_3\overline{S}$), jointly with belite, ferrite and other minor components [8–14]. Cement nomenclature will be used hereafter: C = CaO, S = SiO_2, A = Al_2O_3, F = Fe_2O_3, T = TiO_2, $\overline{S}$ = SO_3, $\overline{C}$ = CO_2 and H = H_2O.

CSA cements are prepared by mixing the clinker with different amounts of a calcium sulfate set regulator such as gypsum ($C\overline{S}H_2$), bassanite ($C\overline{S}H_{0.5}$) or anhydrite ($C\overline{S}$), or mixtures of them. Furthermore, it is possible to modify the hydration process of CSA cements not only by its composition, but also by the selection of different quantities [15] or sources of calcium sulfate [5,16–19].

During the hydration process [18,19], three main issues take place: (i) dissolution of crystalline anhydrous phases, (ii) appearance of new phases such as crystalline ettringite (a.k.a. AFt), and amorphous gels such as aluminate hydroxide hydrate (AH_3); and (iii) consumption of free water. The precipitation can be summarized as follow: yéelimite in presence of a sulfate source (gypsum, bassanite or anhydrite) and in aqueous medium will form ettringite and gibbsite (AH_3), according to Eqs. (1)–(3), respectively. AH_3 precipitates as a poorly-crystallized or amorphous phase [2]. Most of the hydration heat is released during the first 24 h of hydration [20]. Furthermore, bassanite will also react with water to form gypsum and will release heat, according to Eq. (4).

* Corresponding author. Tel.: +34 952131992; fax: +34 952131870.
E-mail address: isantacruz@uma.es (I. Santacruz).

http://dx.doi.org/10.1016/j.cemconcomp.2014.08.003
0958-9465/

$$C_4A_3\bar{S} + 2C\bar{S}H_2 + 34H \rightarrow C_6A\bar{S}_3H_{32} + 2AH_3\text{-gel} \quad (1)$$

$$C_4A_3\bar{S} + 2C\bar{S}H_{0.5} + 37H \rightarrow C_6A\bar{S}_3H_{32} + 2AH_3\text{-gel} \quad (2)$$

$$C_4A_3\bar{S} + 2C\bar{S} + 38H \rightarrow C_6A\bar{S}_3H_{32} + 2AH_3\text{-gel} \quad (3)$$

$$C\bar{S}H_{0.5} + 1.5H \rightarrow C\bar{S}H_2 \quad (4)$$

Ettringite is the main crystalline hydration product together with amorphous aluminum hydroxide. Once the sulfate source (gypsum, bassanite or anhydrite) is depleted and there is enough free water available, monosulfate also known as AFm ($C_4A\bar{S}H_{12}$) [21] is formed according to Eq. (5). Hence, the amount of added calcium sulfate strongly modifies the ettringite to monosulfate mass ratio and the water demand to complete full hydration [6,22]. In addition, the amount of ettringite is affected by the reactivity of calcium sulfate (solubility and dissolution rate) at early ages [6]. Hence, the selection of the sulfate source is a key issue to achieve the desired properties. Furthermore, depending on the minor phases present in CSA cements, other hydration products may occur such as C–S–H gels, stratlingite, katoite, monocarboaluminate or hydrogarnet [4,17,23].

$$C_4A_3\bar{S} + 18H \rightarrow C_4A\bar{S}H_{12} + 2AH_3 \quad (5)$$

The control of the rheological behavior [15] of cement pastes is a key point [24–26] to improve the workability of mortars [27] and to obtain more homogeneous mixtures and hence, improved mechanical properties in general and compressive strengths in particular. In addition, the setting evolution of cement pastes can be also followed at very early hydration times by following their viscosity values.

The objective of this work is to study the effect of different sulfate sources on the hydration of CSA cements at early ages, including the evolution of phase assemblages, rheological behavior (very early ages), evolved heat and microstructure. Finally, the mechanical strength values of the corresponding mortars have been correlated to those variables and the role of the sulfate source is discussed.

2. Materials and methods

2.1. Materials

2.1.1. Preparation of anhydrous cements

Calcium sulfoaluminate clinker, industrially produced in China, and commercial micron natural gypsum ($C\bar{S}H_2$) both marketed by BELITH S.P.R.L. (Belgium) were used as raw materials. Bassanite ($C\bar{S}H_{0.5}$) and anhydrite ($C\bar{S}$) were prepared by heating the as-received gypsum at 90 °C for 48 h and at 700 °C for 1 h, respectively. Calcium sulfoaluminate cements were prepared by mixing clinker with 25 wt% of each of the three different sulfate sources. Depending on the sulfate source, gypsum, bassanite or anhydrite, the corresponding cements will be named hereafter G, B or A, respectively. The elemental analysis of both commercial raw materials (CSA clinker and gypsum) determined by X-ray fluorescence (XRF) was given elsewhere [24]. The Blaine fineness values for all the samples were very close to 450 m^2/kg.

2.1.2. Preparation of cement pastes

Cement pastes were prepared with distilled water using two different water/cement (w/c) mass ratios: 0.50 and 0.65. A commercial polycarboxylate-based superplasticizer, Floadis 1623 (Adex Polymer S.L., Madrid, Spain), with 25 wt% of active matter, was added to water (0.015 and 0.020 wt% active matter referred to the total solids content) for selected pastes prepared with bassanite. Pastes, prepared in an agata mortar, were poured into a hermetically closed polytetrafluoroethylene (PTFE) cylinder shape mold during the first 24 h at 20 ± 1 °C. A drawing of this mold is shown in Fig. 1a. Then, samples were taken out and stored within deionized water at 20 ± 1 °C. Hardened pastes were characterized after 1, 3, 7, 28 and 180 days of hydration. After the given time, pastes were divided into two fractions to perform further characterization, as detailed just below.

2.1.3. Stopping hydration of cement paste

One fraction of the paste cylinder was milled into fine powder with an agate mortar prior to stopping hydration. The stopping procedure consisted on filtration in a Whatman system (70 mm diameter Whatman filter with a pore size of 2.5 μm and a Teflon support) with acetone (Prolabo S.A.) twice and finally with diethyl ether (Prolabo S.A.). The stopped-hydration samples were stored in a desiccator to avoid further hydration and any possible carbonation/alteration [28,29].

2.2. Characterization

2.2.1. Rheological behavior

Cement pastes were mechanically stirred with helices according to UNE-EN 196-3:2005+A1:2008 standard procedure prior to rheological characterization. Rheological measurements of fresh pastes were carried out using a viscometer (Model VT550, Thermo Haake, Karlsruhe, Germany) with a serrated coaxial cylinder sensor, SV2P, provided with a solvent trap to reduce evaporation. Two different measurements were performed. On the one hand, flow curves were obtained under controlled rate (CR) measurements. Ramp times of 6 s were recorded in the shear rate range between 2 and 100 s^{-1}, for a total of 12 ramps. A further decrease from 100 to 2 s^{-1} shear rate was performed by following the same ramp times. On the other hand, viscosity vs. time measurements at a fixed shear rate of 4 s^{-1} were also performed for a maximum time of 150 min, which depended on the setting time of every sample. Prior to any rheological measurement, pastes were pre-sheared for 30 s at 100 s^{-1} and held at 0 s^{-1} for 5 s in the viscometer.

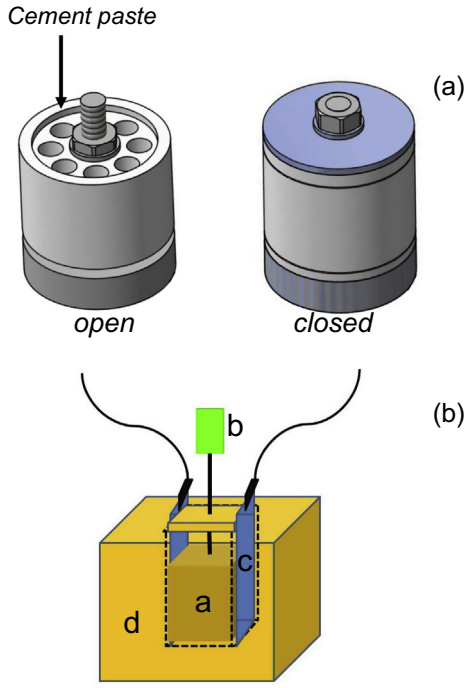

Fig. 1. (a) Hermetically closed PTFE cylinder shape recipient to prepare cement pastes. (b) Home-made cell to impedance spectroscopy measurement: a – Sample; b – Thermocouple; c – Stainless steel electrodes; d – expanded polystyrene container.

2.2.2. Setting time

The setting time of every paste was determined using the Vicat test method according to UNE-EN 196-3:2005 + A1:2008. The corresponding initial setting times are shown in Table S1, given as Supplementary information.

2.2.3. Laboratory X-ray powder diffraction (LXRPD)

LXRPD studies were performed on anhydrous materials and hydrating pastes at 1, 3, 7, 28 and 180 days. Both in-situ transmission (fresh pastes up to 3 h of hydration) and reflection (on pastes after stopping hydration) geometries modes were used.

(i) *Transmission geometry:* This mode was used to study the in-situ hydration of fresh pastes during the first 3 h. All the anhydrous cements were mixed with 15 wt% SiO_2 (99.99%, Sigma–Aldrich, St. Louis, MO, USA) as an internal standard [30]. Data were collected on a PANalytical EMPYREAN automated diffractometer. Powder patterns were recorded in θ–θ transmission configuration by using a focusing mirror and the PIXcel 3D detector (working in 1D mode) with a step size of 0.013° (2θ). The powder patterns were recorded between 5° and 70° in 2θ with a total measuring time of 10 min. The samples were prepared ex-situ and immediately placed into the holders of the diffractometer between two Kapton films. Anhydrous samples with the internal standard were also measured to obtain the initial phase assemblage (0 min). The absorption factors were experimentally measured by comparison of the direct beam with and without sample. The amount of sample loaded in the sample holders was controlled [31] to obtain a total absorption, $\mu t \sim 1$, which corresponds to an absorption factor of ~2.7.

(ii) *Reflection geometry:* This mode was used to study the hydration of the pastes at 1, 3, 7, 28 and 180 days (after stopping hydration). Patterns were recorded on an X'Pert MPD PRO diffractometer (PANalytical) using strictly monochromatic Cu Kα1 radiation (λ = 1.54059 Å) [Ge(1 1 1) primary monochromator] and working in reflection geometry (θ/2θ). The X-ray tube worked at 45 kV and 40 mA. The optics configuration was a fixed divergence slit (1/2°), a fixed incident antiscatter slit (1°), a fixed diffracted antiscatter slit (1/2°) and X'Celerator RTMS (Real Time Multiple Strip) detector, working in scanning mode with maximum active length. Data were collected from 5° to 70° (2θ) during ~2 h. The samples were rotated during data collection at 16 rpm in order to enhance particle statistics. A polished polycrystalline quartz rock was used as secondary standard placed on the diffractometer in the very same orientation. The suitability of this quartz-rock was tested against NIST standard reference material SRM-676a (α-Al_2O_3).

2.2.4. LXRPD data analysis

LXRPD patterns of anhydrous powders, hydrated pastes and the external standard were analyzed by the Rietveld methodology as implemented in the GSAS software package [32] to extract the Rietveld quantitative phase analysis (RQPA). The refined overall parameters were cell parameters, zero-shift error, peak shape parameters, and phase scales. Peak shapes were fitted by using the pseudo-Voigt function [33] corrected for axial divergence [34].

The Amorphous and Crystalline non-quantified (ACn) contents were determined by external standard method (G-factor) from LXRPD in reflection mode data [35]. ACn content computes not only the amorphous fraction but also any not-computed crystalline phase and any misfit problem (for instance the lack of an adequate structural description for a given phase).

2.2.5. Thermal analysis

Differential thermal (DTA) and thermogravimetric (TGA) analyses were performed in a SDT-Q600 analyzer from TA instruments (New Castle, DE) for a ground fraction of every paste after stopping hydration as described above. The temperature was varied from room temperature (RT) to 1000 °C at a heating rate of 10 °C/min. Measurements were carried out in open platinum crucibles under nitrogen flow. The weighed loss from RT to 600 °C was assumed to be water (free and chemically bounded water) and that from 600 to 1000 °C was considered as CO_2. Table S2 includes these data, given as Supplementary information.

2.2.6. Impedance spectroscopy

A home-made cell which measures simultaneously both impedance spectroscopy and temperature of cement pastes was used during the first 10 h of hydration. This consists on a hermetic cell with a prismatic shape (30 × 30 × 50 mm) made of expanded polystyrene (EPS) and two stainless steel electrodes located inside. A drawing of this cell is shown in Fig. 1b. The cell was filled up with 60 g of cement paste. Impedance spectra were obtained at RT using a frequency response analyzer (Solartron 1260) in the 5 Hz to 1 MHz frequency range with an ac perturbation of 200 mV. Electrical data were taken every 15 min. Impedance spectra were analyzed with ZView program [36]. Temperature values were collected with a *K* type thermocouple (resolution of 1 °C) located between electrodes, in the middle of the cell. These studies took over 10 h to be completed.

2.2.7. Scanning electron microscopy (SEM)

The fracture cross-sections of gypsum, bassanite and anhydrite cement pastes at 1 day of hydration were observed by scanning electron microscopy, SEM, (JEOL-JSM-840, Tokyo, Japan). Prior to SEM observation, the hydration of those samples was stopped by immersing them in isopropanol for 3 days and then heated at 40 °C for 24 h. The samples were gold sputtered.

2.2.8. Compressive strength and dimensional stability tests

Standard mortars were prepared with water/CSA/sand ratios of X/1/3 (X depends on the *w*/*c* ratio) and mechanically homogenized according to UNE-EN196-1. Cubic samples of 30 × 30 × 30 mm for all matrix were cast in a jolting table (Model UTCM-0012, 3R, Montauban, France) with a total of 120 knocks. For a better homogenization, molds were half cast and knocked 60 times. After that, they were fully cast and another 60 knocks were performed. The casts were cured at 20 ± 1 °C and 99% RH during 24 h. After that time, samples were demolded and cured within a tap water bath at 20 ± 1 °C until measurements were performed. The compressive strength of the corresponding mortars were measured at 1, 3, 7, 28 and 180 days and the reported values are the average of three broken cubes in a compression press (Model Autotest 200/10 W, Ibertest, Madrid, Spain), according to EN196-1 and at a rate of 1.5 MPa s^{-1}. The measured compressive strength values were corrected by a factor of 1.78 to take into account the difference in area with standard prisms (40 × 40 × 160 mm).

The dimensional stability of the studied CSA mortars was measured with standard prismatic samples (40 × 40 × 160 mm) by applying the following equation: $\Delta L(\%) = \frac{L_f - L_o}{L_o} \times 100$, being L_f the measured length at a given time and L_o the initial length. The later was taken just after demolding and prior to immersion in water. The preparation and curing procedure of these specimens were the same as detailed before. The dimensional stability of Ordinary Portland mortar (from CEM-I 52.5R Portland cement, marketed by Italcementi Group (FyM, Málaga, Spain)) and prepared at water/cement/sand ratios of 0.50/1/3) was also measured, under same conditions, for the sake of comparison.

3. Results and discussion

Prior to the rheological characterization, the initial setting time of all pastes, Table S1, was determined for cement performance characterization and to avoid any damage of the viscometer sensor.

Bassanite (B) pastes show the fastest initial setting time, 20 min, independently of the water content or the addition of a small amount (0.020 wt%) of superplasticizer (SP). Anhydrite (A) pastes show the slowest initial setting time, being even larger for $w/c = 0.65$. Gypsum (G) pastes show intermediate initial setting time values, which was independent of the water content. This is in agreement with the trend in solubility of these calcium sulfate sources in water (0.88, 0.24 and 0.21 g/100 mL for bassanite, gypsum and anhydrite, respectively, at 20 °C).

It has to borne in mind that A-pastes actually have lower water/solid ratios, as this sulfate source does not have any crystallization water. Taking into account the crystallization water contents of gypsum and bassanite, the actual water/solid ratios for G-pastes are 0.58 and 0.74, for B-pastes are 0.52 and 0.68, while for A-pastes remain 0.50 and 0.65.

Fig. 2a shows the flow curves of all the studied pastes. All these fresh pastes show shear thinning behavior and a rheopectic cycle. Bassanite pastes show both the highest viscosity values and the largest rheopectic cycle. Since our objective is to study the effect of the calcium sulfate source on hydration including compressive strengths of the corresponding mortars, similar rheological behavior, and in particular, similar viscosity values are required for all the pastes. In order to achieve that, different amounts of SP were added to B-pastes with the consequent reduction in viscosity. When a very small amount of SP, 0.015 wt%, was added to the bassanite cement paste with $w/c = 0.50$, it exhibited a considerable diminishing in viscosity (from 4.7 to 1.6 Pa s at 50 s^{-1}) and in the rheopectic cycle (from −13650 to −3500 Pa s^{-1}); nevertheless, this is not enough to show similar rheological behavior than G and A pastes, which show viscosity values of 1.0 and 0.8 Pa s at 50 s^{-1}, respectively, and small rheopectic cycles (−800 and −280 Pa s^{-1}, respectively), Fig. 2a. However, when 0.020 wt% of SP is added to the bassanite-paste, the rheological behavior of this paste at very early ages is similar to those prepared with gypsum or anhydrite ($w/c = 0.50$), showing even lower viscosity, 0.6 Pa s at 50 s^{-1}, and an intermediate rheopectic cycle, −440 Pa s^{-1}. Pastes with a w/c ratio of 0.65 are also shown in Fig. 2a for the sake of comparison, and show lower viscosity values than those with 0.50, as expected. Furthermore, these fresh pastes prepared with bassanite and anhydrite ($w/c = 0.65$) show very similar rheological behaviors. B-pastes with $w/c = 0.65$ with and without SP were not further characterized due to the poor mechanical properties of the corresponding pastes/mortars.

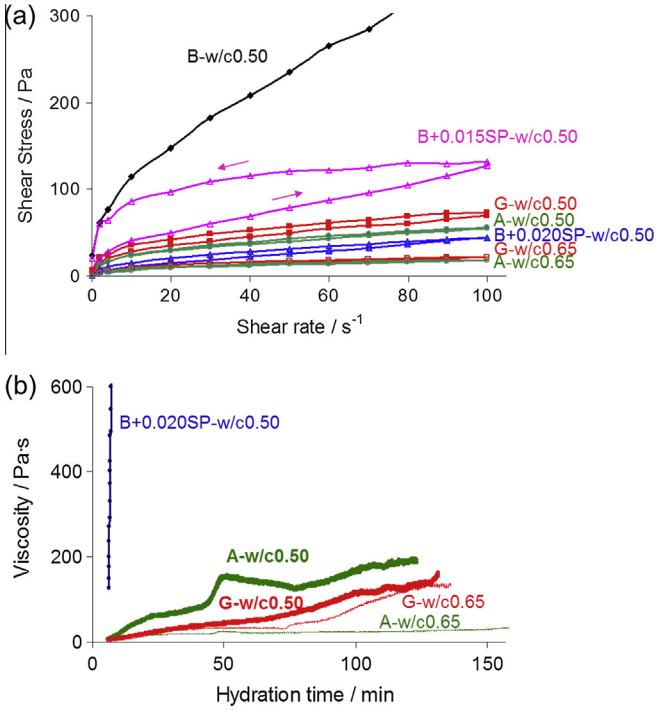

Fig. 2. (a) Flow curves and (b) viscosity vs. time curves at a shear rate of 4 s^{-1} for all the studied cement pastes.

Fig. 2b shows the evolution of viscosity with time for all the studied pastes at a shear rate of 4 s^{-1}. This selected shear rate is low enough for not destroying the structure and high enough for obtaining trustable data. The viscosity of all these pastes increases with time, as expected. B-paste with 0.020 wt% SP ($w/c = 0.50$) showed relatively low initial viscosity values (see Fig. 2a) but its viscosity showed a sharp increase and achieves 600 Pa s in less than 10 min of hydration. This is related with the quick bassanite dissolution and hence quick ettringite formation [15]. When SP is not added into the bassanite paste, the increasing in viscosity is even faster, so it is not shown in Fig. 2b. The viscosity of gypsum and anhydrite pastes increases at slower pace than that of bassanite pastes, where the A-paste is the slowest one for $w/c = 0.65$, within the first 130 min of hydration. Although G and A pastes with $w/c = 0.65$ show similar initial viscosity values, the gypsum pastes showed a marked increase of viscosity after 75 min.

This is a complex process where different parameters are evolved. The hydration of cement pastes is a process of ions dissolution, ions saturation, and a final precipitation of new phases, such as ettringite. From the rheological point of view, the dissolution of cement phases would reduce the solids loading which may decrease the viscosity; however, the increase in ions content would decrease the electric double layer around the particles and hence will enlarge the viscosity; in addition, the presence of new solid phases also would increment the viscosity, although the ions concentration (ionic conductivity) would be lower. Moreover, ettringite particles usually show a prismatic/needle shape that it is known to yield a more dramatic effect on the viscosity than spherical particles [37].

The evolution of both conductivity and temperature is shown in Fig. 3a and b, respectively, for pastes with $w/c = 0.50$. These measurements have been performed within the first 10 h of hydration using the device shown in Fig. 1b. All pastes show a specific value of conductivity at the beginning of the hydration between 0.020 and 0.030 S cm^{-1}. In all pastes, the conductivity decreases after a few minutes of hydration. At that time, the temperature starts to increase up to a maximum value which is coincident with a point close to the minimum value of conductivity. Bassanite pastes with and without 0.020 wt% SP show similar behavior. Differences on conductivity and temperature between G, B and A pastes start just after 20 min of hydration. Both bassanite pastes release high amounts of heat (these pastes achieved temperatures ~80 °C) in a very short time (~100 min), and the conductivity is negligible just after 200 min of hydration. This very large amount of released heat may be explained by the initial dissolution of bassanite and precipitation of gypsum. This *new* gypsum progressively re-dissolves and ettringite is formed. G-paste shows an initial conductivity similar to that for B-pastes (~0.03 S cm^{-1}); however, conductivity and temperature are kept constant within the first hour of hydration for G-pastes. Furthermore, a maximum temperature of only 45 °C is observed after 130 min, where the conductivity is still 0.015 S cm^{-1}, which is ~0.0025 S cm^{-1} after 10 h. Finally, anhydrite pastes show the lowest initial conductivity, ~0.020 S cm^{-1}, and it starts to decrease after 120 min. In addition, the maximum temperature, 52 °C, happens after 270 min; this is due to the low solubility of anhydrite. After that time, the system continues with the hydration and its conductivity is almost negligible after 350 min. Summarizing, the temperature increases firstly for bassanite pastes, secondly for gypsum pastes, and finally for

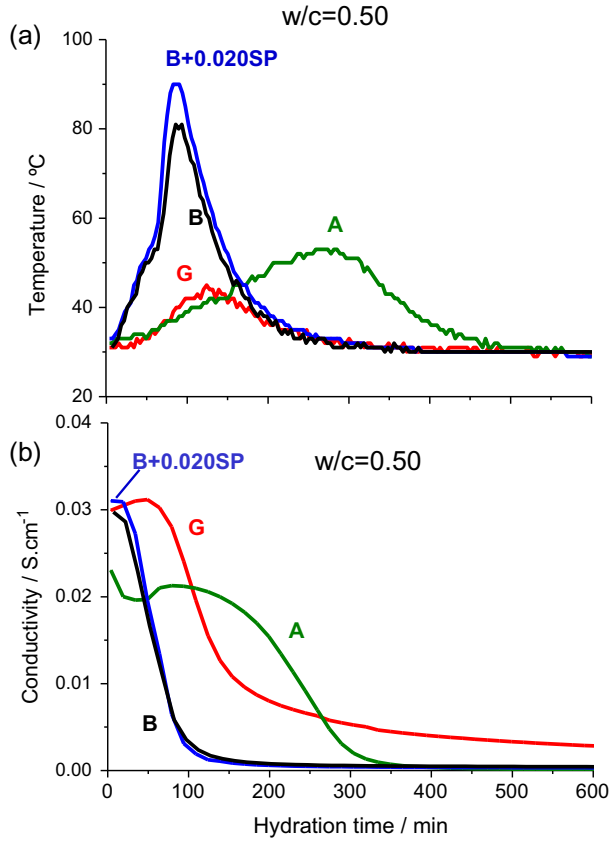

Fig. 3. (a) Temperature and (b) conductivity evolution of fresh pastes within the first 600 min hydration.

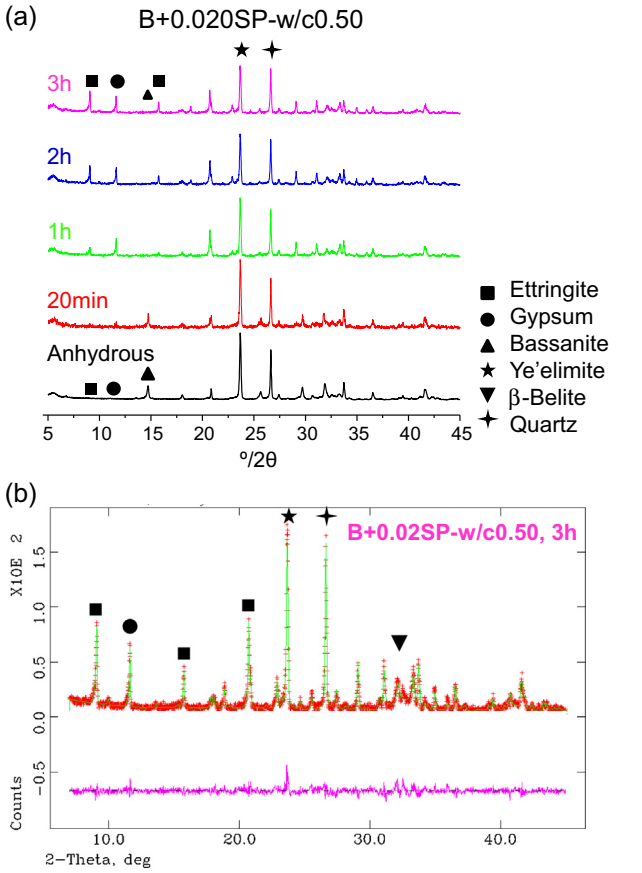

Fig. 4. (a) LXRPD diffractograms of B-w/c0.50 with 0.020 wt% SP at different hydration times (from 20 min to 3 h) measured in transmission mode. The diffractogram of the anhydrous paste is shown for the sake of comparison. (b) Diffractogram (transmission) with a Rietveld analysis of the same paste after 3 h of hydration, where the peaks of the main phases are marked.

anhydrite pastes, following the trend of solubility; this is in agreement with the setting time of the corresponding pastes (Table S1). A-w/c0.50 paste shows lower initial ionic conductivity than G-w/c0.50; this may be also related with its lower initial sulfate dissolution. All these effects might explain the higher viscosity values with time of A-w/c0.50 pastes when compare with G-w/c0.50 pastes (Fig. 2b). In addition, its concentration of ions decreases at a slower pace, being higher than the corresponding value for G-paste between 100 and 260 min of hydration.

LXRPD measurements in transmission mode were performed for a better understanding of the early cement hydration behavior. Fig. 4a shows the raw patterns of B-paste with 0.020 wt% SP at different hydration times, including the anhydrous B-cement. From this figure, the evolution of different phases is clear; bassanite is still present after 20 min of hydration but it has disappeared at 1 h. Part of the bassanite has been transformed on gypsum after 20 min, and the latter is present even after 3 h of hydration in a large amount. In addition, yéelimite is slightly decreasing with time and ettringite content up to 1 h of hydration. This is in concordance with Fig. 3a and b, concerning ion conductivity and temperature. The values for the Rietveld Quantitative Phase Analysis (RQPA) including ACn and free water (FW) for all pastes measured in transmission mode (from 0 min to 3 h of hydration) are shown in Tables 1–3 and S3, the latter provided as Supplementary information. The values obtained from internal standard method encompass not only ACn but also FW (water chemically not bounded) and are expressed as a single value in Tables 1–3 and S3. This is due to the inability of the internal standard methodology to distinguish between two different not diffracting phases. Fig. 4b shows the Rietveld plot for B-paste with 0.020 wt% SP after 3 h of hydration. From these tables, the transformation of bassanite into gypsum can be followed, and the dissolution of gypsum and anhydrite with time, and the formation of new phases, mainly AFt.

Table 1
Rietveld quantitative phase analysis results in weight percentage (including ACn and FW) for G-pastes with $w/c = 0.50$ as a function of hydration time obtained by in-situ LXRPD (up to 3 h) in transmission geometry.

	0 min	20 min	1 h	2 h	3 h
$C_4A_3\bar{S}$	23.4(2)	24.5(4)	23.5(3)	21.6(3)	21.0(3)
$C\bar{S}H_2$	14.9(2)	16.1(4)	15.0(3)	13.8(3)	13.8(3)
β-C_2S	6.4(6)	7.5(1)	9.7(9)	8.3(9)	8.1(9)
Minor phases[a]	4.4(4)	1.8(4)	1.6(2)	1.7(2)	1.8(2)
ACn + FW	50.9	48.0	44.8	46.0	46.0
AFt	0.0	1.6(5)	4.9(3)	8.2(4)	8.9(4)
Gibbsite	0.0	0.5(3)	0.5(2)	0.4(2)	0.4(2)
SUM	100.0	100.0	100.0	100.0	100.0

[a] Overall amount of cement crystalline minor phases: $CaTiO_3$ and MgO.

Tables S4–S7, provided as Supplementary information, show the values of RQPA for gypsum and anhydrite pastes measured in reflection mode, from 0 to 180 days of hydration. These results include the ACn content obtained through the external standard methodology as described above. These tables also include FW which have been obtained by comparing weight losses from RT to 600 °C from DTA–TGA data, Table S2, and the theoretical total weight loss. It is known that the hydration reaction of belite may be quite different in CSA cements [15,24] than that in OPC. And, after a careful examination of the pastes after 180 days of

Table 2
Rietveld quantitative phase analysis results in weight percentage (including ACn and FW) for B-paste with $w/c = 0.50$ as a function of hydration time obtained by in-situ LXRPD (up to 3 h) in transmission geometry.

	0 min	20 min	1 h	2 h	3 h
$C_4A_3\bar{S}$	25.2(2)	24.7(5)	23.4(3)	20.4(3)	20.2(3)
$C\bar{S}H_2$	0.0	5.3(4)	14.3(3)	12.6(3)	12.6(3)
$C\bar{S}H_{0.5}$	13.3(2)	6.5(4)	0.0	0.0	0.0
β-C_2S	2.5(5)	2.9(9)	5.3(8)	5.2(8)	4.7(6)
Minor PHASES[a]	2.7(3)	1.2(4)	1.6(2)	1.7(2)	1.6(2)
ACn + FW	56.3	57.9	48.0	48.8	47.6
AFt	0.0	0.8(4)	7.0(3)	10.9(4)	12.9(4)
Gibbsite	0.0	0.7(4)	0.4(2)	0.4(2)	0.4(2)
SUM	100.0	100.0	100.0	100.0	100.0

[a] Overall amount of cement crystalline minor phases: $CaTiO_3$ and MgO.

Table 3
Rietveld quantitative phase analysis results in weight percentage (including ACn and FW) for A-pastes with $w/c = 0.50$ as a function of hydration time obtained by in-situ LXRPD (up to 3 h) in transmission geometry.

	0 min	20 min	1 h	2 h	3 h
$C_4A_3\bar{S}$	24.6(2)	24.2	23.0(3)	22.8(3)	20.4(3)
$C\bar{S}$	13.8(2)	14.2(4)	13.8(3)	13.2(3)	12.1(3)
β-C_2S	4.2(8)	4.4(1)	4.2(9)	5.1(9)	4.0(9)
Minor phases[a]	2.6(4)	0.9(4)	1.3(2)	1.3(2)	1.2(2)
ACn + FW	54.8	54.8	55.1	51.6	54.2
AFt	0.0	0.9(3)	2.2(3)	5.6(3)	7.8(3)
Gibbsite	0.0	0.6(3)	0.4(2)	0.4(2)	0.3(2)
SUM	100.0	100.0	100.0	100.0	100.0

[a] Overall amount of cement crystalline minor phases: $CaTiO_3$ and MgO.

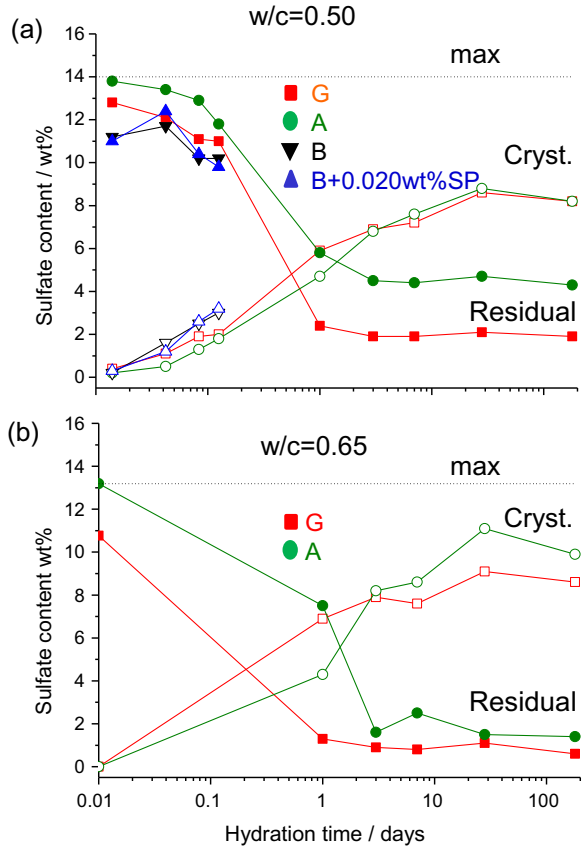

Fig. 5. Weight percentage of SO_4^{2-} groups as a function of time, (a) $w/c = 0.50$, (b) $w/c = 0.65$. "Residual" stands for the remaining gypsum and $C_4A_3\bar{S}$ contents, and "Cryst." stands for crystallized ettringite, both expressed as SO_4^{2-} groups percentage.

hydration, no crystalline products arising from the hydration of belite were observed (portlandite, stratlingite or katoite), although the amount of this phase has slightly diminished. This behavior may be due to its very low degree of reaction.

B-pastes were not studied at later ages by LXRPD in reflection mode because the hydration reactions happen very fast and hence both pastes and mortars show very short setting time. Due to this fact, heterogeneous mortars are produced, which consequently will show poor mechanical performance values.

Table S2 includes weight loss values measured from 600 °C to 1000 °C, from DTA–TGA to clarify any potential carbonation process. It can be observed that, up to 180 days, carbonation process is almost negligible for all the studied pastes. It is worth highlighting that after 180 hydration days small amounts of FW still remains in the pastes, showing no drying effects, see Tables S4–S7. Small amounts (⩽1.5 wt%) of crystalline vaterite ($CaCO_3$) were quantified for G-pastes, confirming that only a very small carbonation has been carried out in these pastes, but not for anhydrite-pastes.

The chemical behavior of sulfates in these systems has been deeply studied through sulfate-containing phase dissolutions and crystallizations with time (normalized to 100 g of CSA cement for the sake of comparison). Fig. 5 shows the evolution of residual sulfate (solid symbols), expressed as percentage of SO_4^{2-} groups (after dissolution/reaction) and crystallized (Cryst.) sulfate (open symbols) for all the samples grouped according to w/c ratio. Data obtained in both transmission and reflection modes have been plotted. The amount of reacted/dissolved sulfate was determined from the disappearance of yéelimite and sulfate source (gypsum, bassanite and anhydrite). This value was subtracted from the initial SO_4^{2-} group content to obtain the residual sulfate amount, shown in Fig. 5. The amount of crystallized sulfate was determined from the appearance of ettringite; silicon-free AFm was only quantified for G-w/c0.65 after 180 days. The dotted lines in Fig. 5 indicate the maximum sulfate that can crystallize. The reactivity of sulfate-bearing phases slightly depends on the w/c addition in G-pastes, as they show almost identical evolutions of dissolved and crystallized sulfate groups, Fig. 5, and its dissolution degree changed from 85% to 95% (for G-w/c0.50 and G-w/c0.65, respectively) due to the higher water content.

The increase of w/c ratio from 0.50 to 0.65 causes a higher dissolution degree in A-phases, i.e. from 70% to 90%, respectively. This produces the precipitation of higher amounts of ettringite (Tables S6 and S7). When comparing gypsum, bassanite and anhydrite pastes in Fig. 5, it can be seen that B-pastes, with or without a small amount of SP, show similar behavior (similar percentages of residual and crystallized sulfate), where the content of crystallized sulfate is higher than that for G and A pastes ($w/c = 0.50$). In addition, A-pastes show the largest residual sulfate content in the range of study. This is in agreement with the conductivity values shown in Fig. 3b, where A-pastes show the lowest values in the first 2 h of hydration. The amounts of crystallized sulfate for G- and A-pastes at $w/c = 0.50$ are very similar, but higher amounts of sulfate groups are crystallized for A pastes at hydration times over 3 days when $w/c = 0.65$. In all cases, about 85% of the dissolved sulfate is crystallized. The rest (15%) may be in pore solution or ACn phase(s).

Fig. 6 shows the amount of crystallized ettringite as a function of time for all the studied pastes, taken from RQPA results. For $w/c = 0.50$ pastes at hydration times lower than 1 day, anhydrite-pastes show the lowest ettringite contents. This is due to the slower rate of dissolution of anhydrite when compared to gypsum or bassanite. However, at hydration times higher than 1 day, AFt

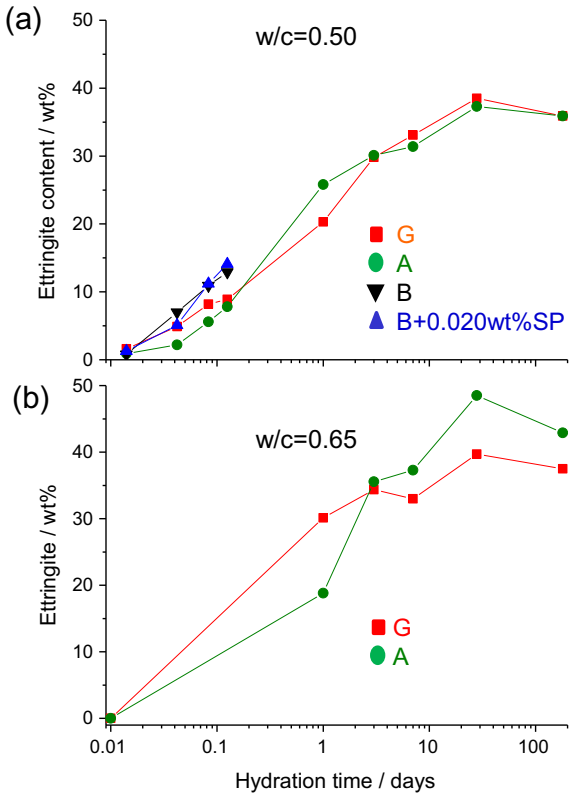

Fig. 6. Ettringite percentage as a function of time, (a) $w/c = 0.50$, (b) $w/c = 0.65$.

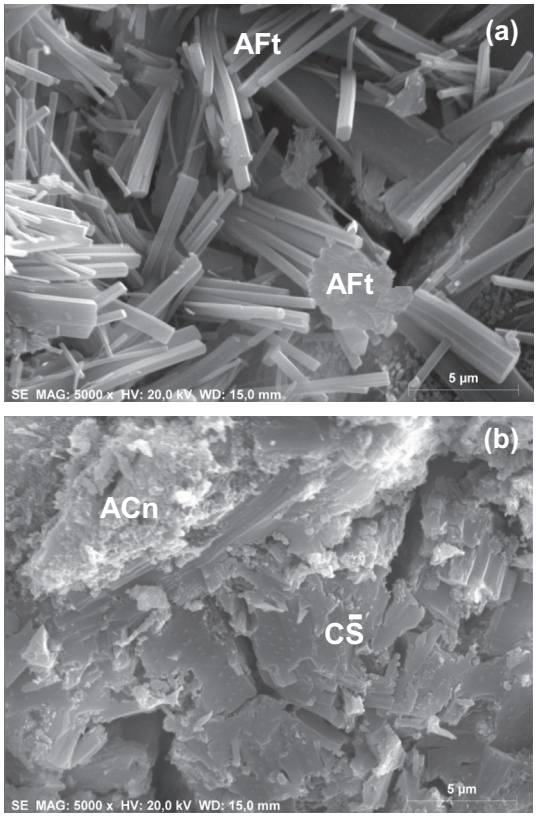

Fig. 7. SEM micrographs of the fracture surface of A-w/c0.50 after 1 day of hydration where (a) ettringite, (b) ACn and anhydrite phases can be observed.

crystallizes at a similar pace in both gypsum and anhydrite pastes ($w/c = 0.50$). Ettringite crystallization resulted to be slightly affected by the water content in gypsum-pastes. However, AFt crystallizes at a higher pace, at hydration times higher than 3 days, in A-pastes by increasing the water content.

Fig. 7 shows selected micrographs of the fracture transversal section of A-paste (w/c0.50) after 1 hydration day. The objective of this figure is to show the presence of ettringite in detail, Fig. 7a, which is known to have a needle shape, and laminar phases, Fig. 7b, that correspond to remaining anhydrite, according to LXRPD, Table S6.

The mechanical behavior of the corresponding mortars was also studied. Fig. 8 gives the compressive strength values of mortars prepared from all pastes grouped according to their w/c ratio and the sulfate source. They were carried out on small cubes as described in the experimental section. From the analysis of the data it is clear that $w/c = 0.50$ mortars always yield higher mechanical strengths than the analogous $w/c = 0.65$ mortars. Furthermore, the role of the sulfate source is also very important. On the one hand, reactions in B-pastes occur very quickly, and their short setting time is enormously sensitive to the degree of homogeneity of the mortars, as mentioned before. The addition of a small amount of SP improves the workability of the mortar but it does not delay appreciably the setting time, hence, both mortars show low mechanical strength values, being slightly higher when the SP is added. On the other hand, and chiefly, the evolution of compressive strength values of gypsum and anhydrite mortars prepared from both types of pastes are in complete agreement with the ettringite formation, see Fig. 6, (the higher ettringite amount, the higher mechanical strength). In the case of gypsum and anhydrite mortars prepared from pastes at $w/c = 0.50$, the formation of ettringite occurred at a greater extent for G-pastes within the first hydration day, hence, G-mortars show higher mechanical strengths at 1 day than those of A-mortars. After 3 days, similar ettringite contents

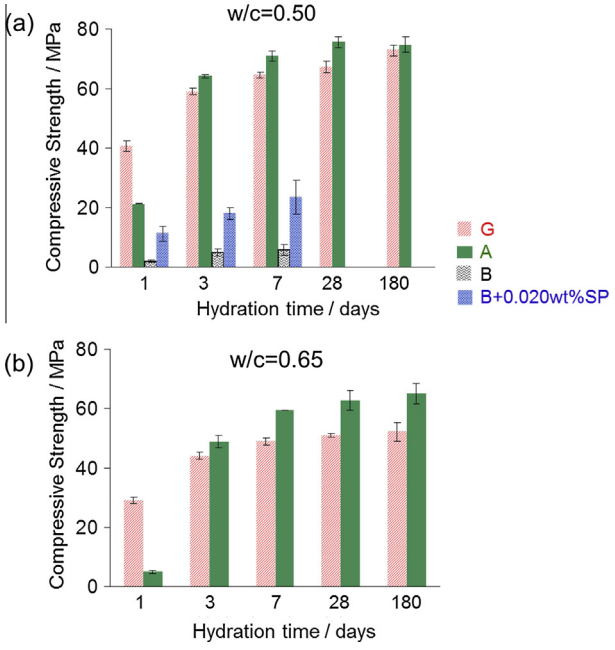

Fig. 8. Compressive strength values of mortars prepared from all pastes at different hydration times (1, 3, 7, 28 and 180 days), (a) $w/c = 0.50$ and (b) $w/c = 0.65$.

were observed for both pastes. However, the setting time for A-pastes was much longer than that for G-pastes, showing a higher plasticity which can better accommodate the precipitation of ettringite. G-w/c0.50 and A-w/c0.50 mortars show similar compressive strengths, being slightly higher for A, likely due to the plasticity.

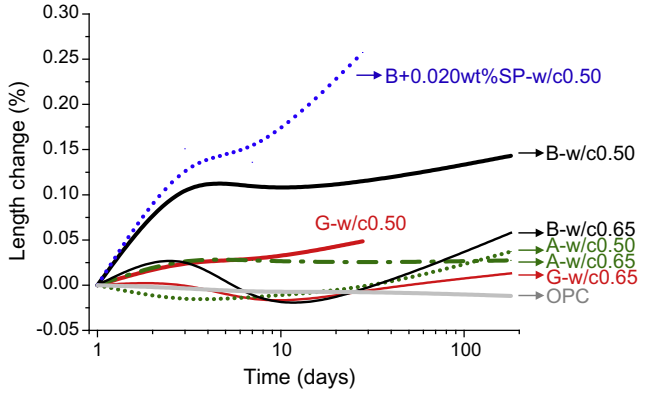

Fig. 9. Length change evolution with time for all the studied mortars.

The longitudinal modifications of the mortars with hydration time were measured and the data are summarized in Fig. 9. This figure represents the percentage of expansion respect to the initial value as detailed in the experimental section. The expansion (or shrinkage) experienced by mortars is mainly related to the nature of pore structure, which affects the mobility of ions and the available space to accommodate new phases. Both adequate deformability and strength values are required to allow expansion without the formation of cracks.

The relatively low expansion values obtained for these mortars agree with previous studies [38]. Our study has revealed that B-mortars do not present enough plasticity to accommodate AFt precipitation with time, consequently higher expansions are observed. On the other hand, gypsum and anhydrite have small effect on the dimensional variation of CSA mortars, since the expansion/shrinkage is almost negligible. The studied OPC mortar experienced almost negligible dimensional changes with time, in agreement with the literature [38].

4. Conclusions

The dissolution rate of the different studied sulfate sources (gypsum, bassanite and anhydrite) is a key point to control the reactions during hydration of CSA cements, and hence the mechanical properties of the corresponding pastes and mortars.

Since bassanite (B) dissolves too quickly in water, all the reactions start too early and hence the initial setting time of the pastes and mortars prepared with bassanite (B-pastes and B-mortars, respectively) is too short to produce homogeneous samples. This will have a dramatic effect onto the mechanical strength values. The addition of a small amount of superplasticizer (SP) (0.020 wt%) improves the workability of the mortar, at very early times, but it does not delay appreciably the setting time, hence, these mortars show low mechanical strength values, being slightly higher when the SP is added. B-mortars do not present enough plasticity to accommodate AFt precipitation with time, consequently higher expansions have been observed.

The dissolution of anhydrite (A) is the slowest of the three systems. Cements and mortars prepared with anhydrite (A-pastes and A-mortars, respectively) show large initial setting times, which also depend on the water content (5 and 11 h for $w/c = 0.50$ and 0.65, respectively). A-w/c0.50 paste shows a low initial ionic conductivity; during the first 10 h of hydration, the ionic concentration decreases at a slow pace, and show low ettringite contents. This produces mortars with compressive strength values (21.0 ± 0.2 MPa) that are lower than those of the corresponding mortars prepared with gypsum (G), G-mortars, (41 ± 2 MPa) after 1 hydration day. However, after 3 hydration days, similar ettringite contents were observed for both pastes. The long setting time of A-mortars provides them with high plasticity to accommodate the precipitation of ettringite. After 3 days of hydration, A-w/c0.50 and G-w/c0.50 mortars show similar compressive strength values, being always slightly higher for A-mortars likely due to its plasticity (for instance, 76 ± 2 and 67 ± 2 MPa for A-w/c0.50 and G-w/c0.50 mortars at 28 hydration days, respectively).

Finally and chiefly, the ettringite contents (determined by RQPA and the G-factor method) in combination with the plasticity of pastes and mortars justify the differences in compressive strength values of the corresponding mortars. The results point out anhydrite as the best sulfate source to be used in CSA mortars for engineering applications when high compressive strength values are needed at hydration time $\geqslant 3$ days. However, if high strength values are demanded at earlier curing ages, gypsum is the best option. Conversely, CSA mortars prepared with bassanite are not recommended unless the setting time could be delayed by the addition of the right type and amount of additives.

Acknowledgements

This work has been supported by Spanish Ministry of Economy and Competitiveness (MINECO) through MAT2010-16213 which is co-funded by European Regional Development Funds (FEDER) and by Junta de Andalucía through P11-FQM-07517 research grants. I. Santacruz thanks a Ramón y Cajal fellowship, RYC-2008-03523.

Appendix A. Supplementary material

Supplementary data associated with this article can be found, in the online version, at http://dx.doi.org/10.1016/j.cemconcomp.2014.08.003.

References

[1] Gartner EM. Industrially interesting approaches to "low-CO_2" cements. Cem Concr Res 2004;34(9):1489–98.
[2] Juenger MCG, Winnefeld F, Provis JL, Ideker JH. Advances in alternative cementitious binders. Cem Concr Res 2011;41(12):1232–43.
[3] Taylor HFW. Cement chemistry. London: Thomas Telford Publishing; 1997.
[4] Aranda MAG, De la Torre AG. Sulfoaluminate cement. In: Pacheco-Torgal F, Jalali S, Labrincha J, John VM, editors. Eco-efficient concrete. Cambridge: Woodhead Publishing Limited; 2013.
[5] Pera J, Ambroise J. New applications of calcium sulfoaluminate cement. Cem Concr Res 2004;34(4):671–6.
[6] Winnefeld F, Barlag S. Calorimetric and thermogravimetric study on the influence of calcium sulfate on the hydration of yéelimite. J Therm Anal Calorim 2009;101(3):949–57.
[7] Odler I. Special inorganic cements. London: Taylor and Francis; 2000.
[8] Chen IA, Juenger MCG. Synthesis and hydration of calcium sulfoaluminate-belite cements with varied phase compositions. J Mater Sci 2011;46(8):2568–77.
[9] Quillin K. Performance of belite-sulfoaluminate cements. Cem Concr Res 2001;31(9):1341–9.
[10] Li GS, Gartner EM. High-belite sulfoaluminate clinker: fabrication process and binder preparation. World Patent Application WO 2006/018569 A2, 2006.
[11] Janotka I, Krajèl U, Mojumdar SC. Performance of sulphoaluminate-belite cement with high $C_4A_3\overline{S}$ content. Ceram Silikaty 2007;51(2):74–81.
[12] Adolfsson D, Menad N, Viggh E, Björkman B. Hydraulic properties of sulphoaluminate belite cement based on steelmaking slags. Adv Cem Res 2007;19(4):133–8.
[13] Álvarez-Pinazo G, Santacruz I, León-Reina L, Aranda MAG, De la Torre AG. Hydration reactions and mechanical strength developments of iron-rich sulfobelite eco-cements. Ind Eng Chem Res 2013;52(47):16606–14.
[14] Wang W, Wang X, Zhu J, Wang P, Ma C. Experimental investigation and modeling of sulfoaluminate cement preparation using desulfurization gypsum and red mud. Ind Eng Chem Res 2013;52(3):1261–6.
[15] García-Maté M, Santacruz I, De la Torre AG, León-Reina L, Aranda MAG. Rheological and hydration characterization of calcium sulfoaluminate cement pastes. Cem Concr Comp 2012;34(5):684–91.
[16] Pelletier-Chaignat L, Winnefeld F, Lothenbach B, Le Saout G, Müller CJ, Famy C. Influence of the calcium sulphate source on the hydration mechanism of portland cement–calcium sulphoaluminate clinker–calcium sulphate binders. Cem Concr Comp 2011;33(5):551–61.

[17] Glasser FP, Zhang L. High-performance cement matrices based on calcium sulphoaluminate-belite compositions. Cem Concr Res 2001;31(12):1881–6.
[18] Sahu S, Havlica J, Tomková V, Majling J. Hydration behaviour of sulphoaluminate belite cement in the presence of various calcium sulphates. Thermochim Acta 1991;175(1):45–52.
[19] Marchi M, Costa U. Influence of the calcium sulphate and *w*/*c* ratio on the hydration of calcium sulphoaluminate cement. In: Proceedings of the 13th ICCC, Madrid, Spain, 2011.
[20] Zhang L, Glasser FP. Hydration of calcium sulphoaluminate cements at less than 24h. Avd Cem Res 2002;14(4):141–55.
[21] Winnefeld F, Lothenbach B. Hydration of calcium sulfoaluminate cements – experimental findings and thermodynamic modeling. Cem Concr Res 2010;40(8):1239–47.
[22] Winnefeld F, Barlag S. Influence of calcium sulfate and calcium hydroxide on the hydration of calcium sulfoaluminate clinker. ZKG Int 2009;62(9):42–53.
[23] Li GS, Walenta G, Gartner EM. Formation and hydration of low-CO_2 cements based on belite, calcium sulfoaluminate and calcium aluminoferrite. In: Proceedings of the 12th ICCC, Montreal, Canada, 2007.
[24] García-Maté M, De la Torre AG, León-Reina L, Aranda MAG, Santacruz I. Hydration studies of calcium sulfoaluminate cements blended with fly ash. Cem Concr Res 2013;54:12–20.
[25] Champenois JB, Dit Coumes CC, Poulesquen A, Le Bescop P, Damidot D. Beneficial use of a cell coupling rheometry, conductimetry, and calorimetry to investigate the early age hydration of calcium sulfoaluminate cement. Rheol Acta 2013;52(2):177–87.
[26] The Rheology of Fresh Concrete. In: Tattersall GH, Banfill PFG, editors. Editorial: Pitman Advanced Publishing Program, First published 1993.
[27] Banfill PFG. Rheology of fresh cement and concrete. Rheol Rev 2006:61–130.
[28] Wang J. Hydration mechanism of cements based on low-CO_2 clinkers containing belite, yéelimite and calcium alumino-ferrite. PhD Thesis. Lille, University of Lille, 2010.
[29] Mechling JM, Lecomte A, Roux A, Le Rolland B. Sulfoaluminate cement behaviours in carbon dioxide, warm and moist environments. Adv. Cem. Res. 2013;26:52–61.
[30] De la Torre AG, Bruque S, Aranda MAG. Rietveld quantitative amorphous content analysis. J Appl Crystallogr 2001;34(2):196–202.
[31] Cuesta A, Álvarez-Pinazo G, García-Maté M, Santacruz I, Aranda MAG, De la Torre AG, León-Reina L. Rietveld quantitative phase analysis from molybdenum radiation powder diffraction. Powder Diffr, in press.
[32] Larson AC, Von Dreele RB. General structure analysis system (GSAS). Los Alamos national laboratory report LAUR; 2000. p. 86–748.
[33] Thompson P, Cox DE, Hasting JB. Rietveld refinement of Debye–Scherrer synchrotron X-ray data from Al_2O_3. J Appl Crystallogr 1987;20:79–83.
[34] Finger LW, Cox DE, Jephcoat AP. A correction for powder diffraction peak asymmetry due to diaxial divergence. J Appl Crystallogr 1994;27:892–900.
[35] Álvarez-Pinazo G, Cuesta A, García-Maté M, Santacruz I, Losilla ER, De la Torre AG, et al. Rietveld quantitative phase analysis of yeelimite-containing cements. Cem Concr Res 2012;42(7):960–71.
[36] Johnson D. ZView: a software program for IES analysis, version 2.8, Scribner Associates Inc, Southern Pines, NC, 2008.
[37] Reología de suspensiones cerámicas. In: Moreno R, editor. Consejo Superior de Investigaciones Científicas (Spanish Council for Scientific Research), 2005. In Spanish.
[38] Chen IA, Hargis CW, Juenger MCG. Understanding expansion in calcium sulfoaluminate–belite cements. Cem Concr Res 2012;42(1):51–60.